ACS Catalysis

Research Article

Cite This: ACS Catal. 2018, 8, 10631−10640

pubs.acs.org/acscatalysis

A Copper-Peptoid as a Highly Stable, Efficient, and Reusable Homogeneous Water Oxidation Electrocatalyst

Totan Ghosh, Pritam Ghosh, and Galia Maayan*

Schulich Faculty of Chemistry, Technion-Israel Institute of Technology, Technion City, Haifa 3200008, Israel

Supporting Information

ABSTRACT: Water electrolysis is among the simplest methods to generate hydrogen, which can be used as a clean and renewable energy source. Within this process, the oxidation of water into molecular oxygen is considered as the bottleneck reaction because it involves the transfer of four electrons toward the oxidation of a highly stable small molecule. Challenges in this area include the development of stable and effective electro- and photocatalysts that utilize readily available metal ions. Herein we report a copper−peptidomimetic complex as an electrocatalyst for water oxidation, which is both highly stable and efficient. Inspired by enzymatic catalysis, which is largely based on intramolecular cooperativity between a metal center and functional organic molecules located on one scaffold, we have designed and synthesized a peptoid trimer bearing a 2,2′-bipyridine (bipy) ligand, an −OH group, and a benzyl group. Both experimental and computational data reveal that binding of Cu^{II} to this peptoid in aqueous medium occurs via the bipy group and two hydroxyl moieties from the solution. Based on a systematic electrochemical study, we show that this complex is an active electrocatalyst for water oxidation in aqueous phosphate buffer solution enabling oxygen evolution at pH 11.5 with a turnover frequency of 5.8 s^{-1} and a Faradaic efficiency of up to 91%. Importantly, this catalyst is highly stable over at least 15 h of electrolysis. Thus, we could reuse it for at least 9 times in 40 min electrolysis experiments, demonstrate that it retains its activity in every experiment, and obtain oxygen evolution with an overall turnover number record (based on moles oxygen to moles catalyst) of >56 in 6 h. Moreover, based on electrochemical experiments, spectroscopic data, and density functional theory-D3 calculations, we identified a key peroxo intermediate and propose an intramolecular cooperative catalytic path for this reaction, which suggests that the −OH group has a major role in the high stability of the complex.

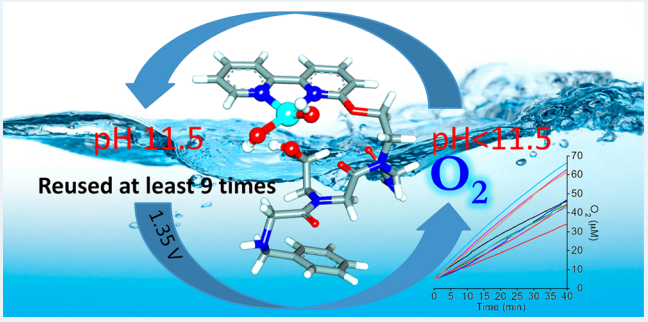

KEYWORDS: *peptide, peptoid, copper, water oxidation, electrocatalysis*

INTRODUCTION

Cooperative catalysis is a key to many successful transformations as it lays in the foundation of enzymatic activity. Enzymatic catalysis is largely based on the cooperativity between binding sites, specifically metal complexes, and nonreacting components that influence reaction barriers and control access to the binding site. This cooperativity leads to the creation of catalytic pockets, which enable enzymes' high specificity and efficiency. Mimicking enzymatic cooperativity by designing intramolecular catalytic systems, in which both the catalytic group(s) and the nonreacting components are tethered in close proximity to each other, is therefore a promising approach to address grand challenges in catalysis, specifically in the catalytic activation of small and stable molecules and bonds. One of the most important challenges in this context is the development of efficient electrocatalysts and photocatalysts for water splitting to molecular oxygen and hydrogen, the later being a renewable and sustainable energy source. The first step in this reaction, water oxidation, is an important step in artificial photosynthesis as it provides the protons and electrons used in reduction reactions to make solar fuels.[1] However, it is also the thermodynamically challenging step both in natural and artificial photosynthesis, $2H_2O \rightarrow O_2 + 4H^+ + 4e^-$ (ΔE° = 1.23 V, ΔG = 113 kcal mol^{-1}).[2] In nature, this transformation is catalyzed by the oxygen-evolving complex (OEC) in photosystem II of green plants and cyanobacteria, exploiting solar energy to drive electron transfer.[3,4] Within this process, a noncatalytic redox active tyrosine residue assists transferring protons and electrons between the catalytic center, a $CaMn_4O_5$ cluster, and the oxidant, a primary donor within photosystem II, and serves as a hydrogen-bonding site to provide H_2O and H^+ shuttle pathways to and from the catalytic Mn site.

One major goal in this field is the development of highly efficient and stable electro- and photocatalysts that are based on earth-abundant transition metals. Thus, water oxidation electrocatalysts from Co,[5] Fe,[6] Ni,[7] Cu,[8] and Mn[9] have drawn great attention in recent years. Among these, significant

Received: September 11, 2018
Revised: September 28, 2018
Published: September 28, 2018

DOI: 10.1021/acscatal.8b03661
ACS Catal. 2018, 8, 10631−10640

advances have been made in the area of Cu-based water oxidation catalysis with a notable breakthrough in the development of simple Cu^{II} complexes as homogeneous electrocatalysts.[8,10] Recently, it was shown that −OH groups within copper-binding ligands have a significant role in facilitating the oxidation of the Cu^{II} center and/or in stabilizing the Cu^{III} oxidation state, thus leading to its enhanced activity.[10c,11] In addition, there were two reports on Cu-peptides as electrocatalysts for water oxidations.[8b,10i] These catalysts were shown to perform with high catalytic rate, albeit no cooperative mode of action was demonstrated in these cases. Moreover, as the peptide backbone is significantly unstable toward harsh oxidation and non-natural pH conditions, development of peptides and proteins as water oxidation catalysts might be limited. We therefore envisioned that the use of rationally designed robust biomimetic scaffolds in which the distance, orientation, and interactions between the active groups can be precisely tuned, in combination with an efficient copper water oxidation electrocatalyst, would enable both optimized efficiency and high catalyst stability.

Peptoids, N-substituted glycine oligomers, are an important class of biomimetic oligomers, to which various side chains, including catalysts and metal-binding ligands, can be incorporated in a specific manner.[12] Moreover, we have previously described efficient intramolecular cooperative catalytic oxidation transformations by a peptoid trimer bearing two different catalytic groups, namely, a 1,10-phenanthroline-based copper complex at the N-terminus, 2,2,6,6-tetramethyl-piperidin-1-yl) oxyl in the respective position and a non-catalytic benzyl group.[13] We showed that the position of the three groups affects the catalytic activity and that the presence of the benzyl group is crucial because it actually enables the intramolecular mode of action leading to the high catalytic efficiency. Herein we adopted a similar approach within a short peptoid trimer containing a bipy group, a very good ligand for copper binding, a hydroxyl group as a proton acceptor site that should improve the efficiency and rate of the reaction, and a benzyl group (Scheme 1), which has a role in the intramolecular cooperativity, as a biomimetic ligand backbone for electrocatalytic water oxidation. We found that this peptoid trimer binds copper in alkaline phosphate buffer via the bipy nitrogen atoms and two −OH groups from the solution in a tetra-coordinated geometry and is highly stable and active electrocatalyst toward water oxidation. A systematic study on the electrocatalytic water oxidation activity of the complex in aqueous phosphate buffer solution revealed oxygen evolution at pH 11.5 with a turnover frequency (TOF) of 5.8 s^{-1}, a Faradaic efficiency of up to 91%, and high catalyst stability over at least 15 h. We also showed that the catalyst retains its activity in at least 9 sequential 40 min electrolysis experiments and obtained oxygen evolution with an overall turnover number (TON) record (for homogeneous copper-based water oxidation electrocatalysts) of >56 in 6 h. Moreover, based on previous studies done by other groups as well as electrochemical experiments, spectroscopic analysis, and density functional theory (DFT)-D3 calculations done here, we could propose an intramolecular cooperative catalytic mode of action for this reaction, demonstrating that the hydroxyl group from the peptoid backbone is a key to the high stability and efficiency of the complex.

Scheme 1. Structures of (a) Peptoid Ligand BPT and (b) the Cu−Peptoid Complex [BPTCu^{II}(OH)$_2$], Which Is Expected To Be Formed in Basic pHs

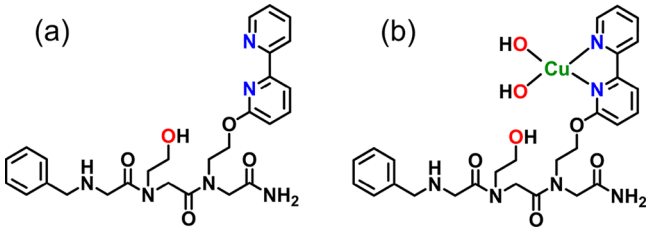

RESULTS AND DISCUSSION

The peptoid **BPT** was synthesized using a solid-phase method[14,15] (see Experimental Section for details), cleaved from the solid support and purified by high-performance liquid chromatography (HPLC, > 95% purity). The molecular weight measured by electrospray mass spectrometry (ESI-MS) was consistent with the mass expected for its sequence (see Supporting Information). This peptoid was treated with copper perchlorate hexahydrate in methanol, and after 2 h of stirring, a blue color solid precipitate was obtained. The precipitate was isolated, washed, and dried. This complex is highly soluble in aqueous solution at various pH conditions. The mass spectra of the Cu-peptoid complex in deionized water (pH = 6.3) showed two peaks at 581.96 and 682.05, which correspond to the complex **BPT**Cu in the absence and presence of one perchlorate ion, respectively (see Figure S3). On the basis of previous reports showing that the combination between bipy and Cu^{II} at pH > 12 affords the complex [Cu(Bipy)$(OH)_2$], which can act as efficient electrocatalyst for water oxidation at pH = 12.5,[8a] we decided to dissolve **BPT**Cu at pH = 12.5 and test its activity as a water oxidation electrocatalyst. Adding the solid metallopeptoid to an aqueous solution at pH = 12.5, however, resulted in the precipitation of a brown solid and the solution became clear. MS analysis indicated that only the metal-free peptoid **BPT** is present in this solution, suggesting the dissociation of the complex at this pH. To explore the stability of this complex in basic conditions, it was further dissolved in aqueous phosphate buffer solutions at pH 8, 10, and 11.5, and characterized by ESI-MS analysis as well as by FT-IR and UV−vis spectroscopy. The MS analysis of the powder copper peptoid complex dissolved in each of these pH conditions revealed three different masses, 582.18, 584.98, and 618.06, which match the masses of **BPT**Cu, (**BPT**Cu + $2H^+$) and [**BPT**Cu^{II}(OH)$_2$], respectively (see Figure S4). The FT-IR spectrum of the complex exhibits the following bands in the 2900−3500 cm^{-1} region: ν (O−H) = 3475 cm^{-1}, ν (N−H) = 3251 cm^{-1}, ν (C−H) = 2964 cm^{-1}, and a band near 1069 cm^{-1}, associated with M-ClO_4 stretching (see Figure S5). The UV−vis spectrum of the peptoid complex in the pH range of 8−11.5 shows a characteristic band at λ_{max} = 322 nm, and is lacking the band at 299 nm, which corresponds to the free bipy-peptoid ligand (see Figure S6). Additionally, the EPR analysis of the complex in basic phosphate buffer solution (frozen) containing 0.5 mM **BPT**Cu^{II}(OH)$_2$ was performed and the spectrum obtained is characteristic of a Cu^{II} system with four hyperfine lines. The simulate spectrum produced the parameters g∥ = 2.28, g⊥ = 2.042 and A∥ = 147G. These clearly imply that there are 2O and 2N atoms coordinating to the Cu^{II} ion[16] (see Figure S7). Collectively, these results suggest that the Cu^{II} ion is bound to the bipy ligand as well as to two −OH units from the solution

DOI: 10.1021/acscatal.8b03661
ACS Catal. 2018, 8, 10631−10640

medium, as accepted in the literature,[17,8a] forming a tetra-coordinated geometry within the metallopeptoid **BPT**$Cu^{II}(OH)_2$ (Scheme 1b). Recently, we have published the crystal structure of a dinuclear Cu^{II} complex from the same peptoid (**BPT**), which was crystallized from acetonitrile solution.[15] In that report, we showed on the basis of experimental spectroscopic data and DFT calculations done with the coordinates taken directly from the CIF file that the structure transforms to the monomeric complex in solution. Here, the experimentally suggested structure of **BPT**$Cu^{II}(OH)_2$ (Scheme 1b) was optimized by DFT-D3 calculations (considering the dispersion correction)[18] at the level of B3-LYP with def2-TZVP for Cu^{II} and def2-SVP for the other atoms as basis sets with unrestricted Hartree−Fock, using turbomole and ORCA (3.0.3) software package. The calculations reported here were executed using the solvent model for water with the coordinates directly taken from the published CIF file (CCDC number 1559281).[15] The optimized structure of [**BPT**$Cu^{II}(OH)_2$] is depicted in Figure 1. As suggested in Scheme 1b, the central metal is four

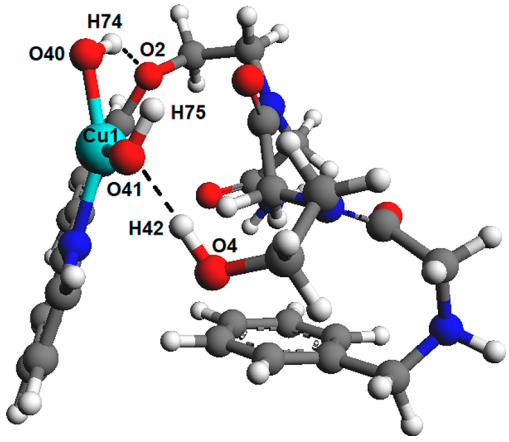

Figure 1. Geometry optimized structure of [**BPT**$Cu^{II}(OH)_2$] (hydrogen bonding is shown in black dotted line).

coordinated, and the bond distances from this center to ligated centers are as follows: Cu (1)-N(7): 2.05 Å, Cu(1)−N(8): 2.10 Å, Cu(1)−O(41): 1.91 Å and Cu(1)−O(40):1.87 Å. The angles are O(41)−Cu(1)−N(7): 92.87°, O(40)−Cu(1)−N(8): 98.48°, N(7)−Cu(1)−N(8): 78.91° and O(40)−Cu(1)−O(41): 96.18°. Interestingly, the −OH moiety from the peptoid side chain forms a strong hydrogen bonding interaction with one hydroxyl moiety that is bound to the Cu^{II} center. In addition, the etheric oxygen atom attached to the bipy ligand is forming hydrogen bonding with the second hydroxyl moiety that is bound to the Cu^{II} center. The hydrogen bond distances are 1.59 Å [O(4)−H(42)···O(41)] and 2.04 Å [O(40)−H(74)···O(2)], respectively, and these stabilize the complex. Overall, our experimental data and DFT-D3 calculations, as well as the relevant literature, indicate that the Cu^{II} ion binds the bipy ligand and two −OH units from the solution medium.

Followed this analysis, we turn our attention to investigate the redox properties of [**BPT**$Cu^{II}(OH)_2$] by cyclic voltammetry (CV) in phosphate buffer at pH = 11.5, 10, and 8. The CVs were obtained under air using a glassy carbon (GC) working electrode and Ag/AgCl reference electrode. On scanning at 100 mV/s from 0 to +1.7 V vs. NHE, the aqueous buffer solutions of the complex exhibited irreversible, pH-dependent oxidation waves in the pH ranges of 8 to 11.5, with the highest catalytic water oxidation peak appearing at pH 11.5 (Figure 2a). Scanning the later solution at 100 mV/s from 0 to +0.8 V

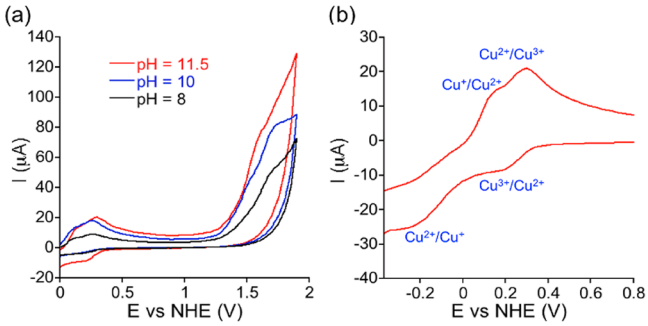

Figure 2. (a) CVs of solutions containing 0.5 mM of the complex [**BPT**$Cu^{II}(OH)_2$] in 0.1 M phosphate buffer at various pH values on a glassy carbon electrode (S = 0.07 cm^2). (b) LSV of the complex [**BPT**$Cu^{II}(OH)_2$] in 0.1 M phosphate buffer at pH = 11.5.

using the linear sweep voltammetry (LSV) technique revealed a well-defined reversible oxidation wave at $E_{1/2}$ = +0.30 V vs. NHE with a peak to peak splitting of ΔE_p= 110 mV corresponding to the formation of a d^8 Cu^{III} (Figure 2b). This oxidation peak is significantly lower than the oxidation potential typically observed for the $Cu^{II/III}$ transition; the minimum potential reported was about 0.52 V vs. NHE.[8] We have previously demonstrated that the incorporation of ruthenium-bipy centers within peptoid oligomers facilitates the $Ru^{II/III}$ process as the oxidation potentials of $Ru(bipy)_3$-peptoids are negatively shifted compare to this of $Ru(bipy)_3$.[12f] The shifts in these cases, however, were rather small (about 50 mV decrease in the $E_{1/2}$), whereas in the case of [**BPT**$Cu^{II}(OH)_2$], we obtained a decrease of about 200 mV. This result suggests an unusual stabilization of the transition state Cu^{III} complex compare to other Cu^{III} complexes that were reported as transition states in electrocatalytic water oxidation. One possible explanation for this unique stabilization could be that the complex forms some hydrogen bonding between the −OH from the ethanolic side chain and the hydroxyl groups bound to Cu. To test this possibility, we have used a copper complex that was prepared from a peptoid trimer similar to **BPT** in which we have replaced the − OH moiety in the ethanolic group by a $-OCH_3$ group.[15] The CV of this complex revealed an Cu^{II}/Cu^{III} oxidation wave at $E_{1/2}$ = +0.50 V vs. NHE (Figure S9). This observation indicates that the −OH group from the ethanolic side chain has a role in facilitating the $Cu^{II/III}$ transition. A second irreversible oxidation, which might be associated with the oxidation of the ligand when bound to Cu or with the oxidation of a stable intermediate,[8c,11] occurs at 1.35 V vs. NHE, leading to catalytic water oxidation. In comparison, unbound peptoid **BPT** dissolved at pH = 11.5 exhibits an irreversible oxidation at 1.75 V, which is not followed by a catalytic water oxidation peak (Figure S10a).

In order to confirm that the catalytic process is homogeneous, we explored whether the catalyst is operating solely in solution or if an active catalyst is being formed and deposited on the electrode surface leading to a heterogeneous process. Thus, we removed the glassy carbon electrode from a solution of [**BPT**$Cu^{II}(OH)_2$] (0.5 mM in 0.1 M phosphate

DOI: 10.1021/acscatal.8b03661
ACS Catal. 2018, 8, 10631−10640

buffer, pH 11.5) after carrying out 30 continuous CV scans from −0.8 to 1.8 V vs. NHE (Figure S11), rinsed it with water (the electrode was not polished), and placed it in fresh 0.1 M phosphate buffer solution at pH 11.5 without [**BPT**$Cu^{II}(OH)_2$]. The CV scan of this solution showed only the blank buffer response (Figure S12). Scanning electron microscope (SEM) images of the working electrode surface before and after 30 continuous CV scans, showed no particle deposited on the electrode surface (Figure S13). The outcome suggests that the catalytic process is homogeneous. In addition, we have examined the scan rate dependence of the oxidation currents in 0.1 M phosphate buffer at pH = 11.5 (Figure 3a)

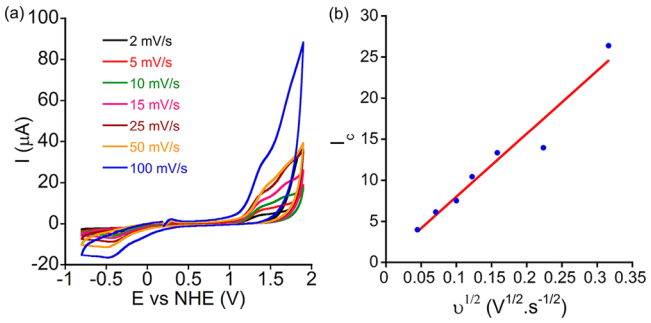

Figure 3. (a) CVs of a 0.5 mM complex solution in different scan rates on a glassy carbon electrode (S = 0.07 cm^2, pH = 11.5, 0.1 M phosphate buffer, background corrected). (b) The catalytic current at 1.35 V vs. NHE plotted against the square root of scan rate (υ).

and obtained a linear fit when plotting the intensity of the catalytic peak current (i_c) against the square root of the scan rate (see Figure 3b). This indicates that the oxidation currents are diffusion controlled and the catalytic process is truly homogeneous.[8b,19]

Evolution of molecular oxygen was investigated by a 2 h controlled potential electrolysis (CPE) experiment at +1.15 V vs. Ag/AgCl reference electrode (1.35 V vs. NHE) with a porous glassy carbon electrode in a 0.1 M phosphate buffer solutions at pH = 8, 10, and 11.5. A significant amount of oxygen was detected only at pH 11.5, and thus, all further CPE experiments were done at this pH. A current of 10 mA/cm^2 was maintained during the electrolysis, which slightly decreased because of a drop in pH by 2.1 units. This is consistent with proton formation in the water oxidation process (Figure S14).[8b] During the CPE experiment, the evolved oxygen was measured in the gas phase by an optical fiber oxygen probe. Within 2 h, the evolved oxygen concentration was increased from 12 μM to 134 μM with [**BPT**$Cu^{II}(OH)_2$] (Figure 4a, red line) and from 11 μM to 18 μM without it (Figure 4a, black line). Overall, 115 μM of oxygen were evolved in the catalytic CPE experiment. This electrolysis experiment was afforded with a charge accumulation of about 12 C (Figure 4b, red line) in the presence of 2.5 μmol [**BPT**$Cu^{II}(OH)_2$], whereas a control experiment run under identical conditions, but without the catalyst (Figure 4b, black line), showed a charge accumulation of only 2.5 C. Based on a $4e^-$ process, the total charge of 9.5 C accumulated in this process and the initial amount of catalyst in solution, the Faradaic efficiency and the catalytic TON were calculated to be 91% and 9 in 2 h, respectively.

Importantly, under these reaction conditions, no precipitation was observed, and the catalyst remained intact as evident from the UV−vis spectrum and CV taken after 2 h of

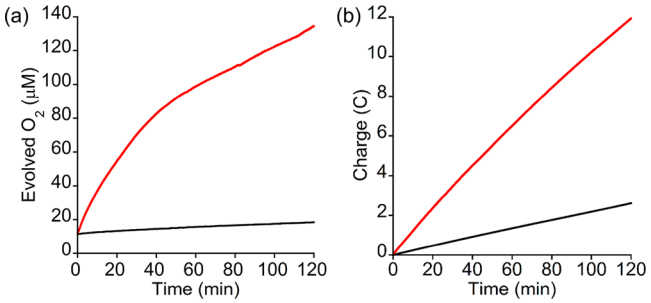

Figure 4. (a) Evolution of O_2 during electrolysis measured with a fluorescence probe and (b) total accumulated charge during control potential electrolysis from a solution containing 0.5 mM catalyst (red lines) and the buffer only (black lines) using a porous GC at 1.35 V vs. NHE. All solutions contained 0.1 M phosphate buffer at pH 11.5.

electrolysis (Figure S15 and S16). Moreover, after adjusting the pH of this solution to 11.5 with 0.1 M aqueous sodium hydroxide solution, it was further subjected to an additional CPE experiment, this time for 15 h, in the same reaction conditions as of the first 2 h experiment (Figure S17−S20). Production of oxygen was observed over a period of 6 h out of the 15 h, as indicated by the nonlinear increase in oxygen evolution detected by the sensor. The total evolved oxygen concentration was 217 μM with the catalyst and 38 μM without it. Overall, 179 μM of oxygen evolved in the catalyzed CPE experiment, which corresponds to a TON of 14.8 in 6 h and to an overall TON of 23.8 in 8 h, based on the amount of the [**BPT**$Cu^{II}(OH)_2$] in solution. We have noticed that most of the oxygen was produced in the first 3 h of the reaction. A closer look at the oxygen production over this 3 h period, as well as over the 2 h period of the initial CPE experiment, revealed that most of the oxygen is actually being produced in the first 40 min of the reaction (see Figure 4a). As the catalyst is highly stable, we assumed that the decrease in activity is a consequence of the decrease in pH. To probe this point, we have prepared a new solution containing 0.5 mM [**BPT**$Cu^{II}(OH)_2$] at pH 11.5 and subjected it to a 50 min electrocatalysis. The CPE experiment was stopped every 10 min, and the pH of the solution was measured before reconnecting to the potentiostat. A distinct decrease in the pH of the solution was observed over this time to pH 10.8 (See Figure S21). As the CPE experiment with [**BPT**$Cu^{II}(OH)_2$] at pH = 10.5 showed only negligible amount of oxygen evolution, we can assume that the reaction slows down significantly at that pH. However, as the catalyst do not show any signs of degradation, we envisioned that we can ideally recycle the catalytic solution by repeating the reaction over and over for a specific period by adjusting its pH to 11.5 each time and thus increase the TON significantly. To explore this possibility, we have prepared a new solution containing 0.25 mM [**BPT**$Cu^{II}(OH)_2$] and performed a continuous CPE experiment by stopping the reaction every 40 min interval with adjusting the pH to 11.5. Keeping the amount of [**BPT**$Cu^{II}(OH)_2$] constant in the bulk solution, we have obtained a TON as high as 56 in 6 h (9 repeating cycles, Figure 5).

In the first six repeating cycles of the experiment, the total amount of oxygen produced in each 40 min reaction was about 30 μM. In the next 3 cycles, however, about 50 μM of oxygen was produced in each cycle (see Figure 5a). We note that as we readjusted the pH by adding sodium hydroxide solution, the

DOI: 10.1021/acscatal.8b03661
ACS Catal. 2018, 8, 10631−10640

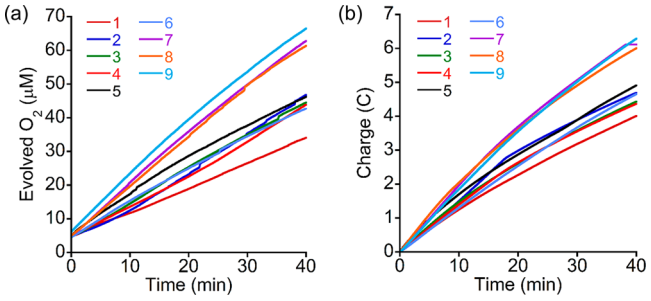

Figure 5. Evolved O_2 (a) and accumulated charge (b) during each 40 min. CPE cycle. Experiments done at 1.35 V vs. NHE with 0.25 mM [**BPT**$Cu^{II}(OH)_2$] at pH = 11.5 in aqueous 0.1 M phosphate buffer solution. Every 40 min the CPE was stopped, and the pH was readjusted to 11.5.

total volume of the catalyst solution in the bulk has increased. As a consequence, after six such additions, the catalytic solution covered a greater area of the porous-carbon working electrode. This effectively led to a larger surface area of the working electrode, enabling more catalyst molecules to react and thus more oxygen and more charge were produced during 40 min electrolysis with the same amount of catalyst. Although the catalyst remains active after 9 cycles, due to the increase in the volume of the reaction mixture it was not possible to continue this CPE experiment further with the same experimental setup. To the best of our knowledge, this is the highest TON reported based on the amount of a copper catalyst in solution. As this catalyst is highly stable, this TON could even increase further by continuing the reaction cycles, and we are currently working toward scaling up this reaction to enable this improvement. Overall, we have developed one of the most highly stable and highly efficient homogeneous copper-based water oxidation electrocatalysts.

It was previously noted that in homogeneous water oxidation, calculating the TON from the ratio of moles oxygen per moles catalyst underestimates the real TON values because only the catalyst near the electrode is involved in the reaction, even though it is being refreshed by diffusion.[8c] A methodology that addresses these considerations in electrocatalytic processes was recently developed for obtaining a more accurate TON and was further adapted to the water oxidation reaction.[20] This TON calculation is based on the apparent rate constant of the reaction, k_{obs}, which could be obtained from a foot-of-the-wave analysis (FOWA).[21] If no side electrochemical events perturbs the catalytic reaction, the reaction is faster than Fv/RT, in which v is the scan rate; thus, it is independent of scan rate and can be described by the following equation:[22]

$$\frac{i}{FS} = \frac{C_p^0\sqrt{D_p \cdot 2kC_A^0}}{1 + \exp\left[\frac{F}{RT}(E - E^0)\right]} \quad \text{(i)}$$

The peak current of the catalyst in the absence of substrate,[23] may serve to calibrate the catalytic response in terms of electrode surface area, S, catalyst concentration, C_p^0, diffusion coefficient, D_p, and scan rate, v.

$$\frac{i_p^{\,0}}{FS} = 0.446 \times C_p^0\sqrt{D_p}\cdot\sqrt{\frac{Fv}{RT}} \quad \text{(ii)}$$

It is thus convenient to observe the variation of

Scheme 2. Proposed Mechanism for Water Oxidation by [BPT$Cu^{II}(OH)_2$] Complex in 0.1M Phosphate Buffer Solution at pH = 11.5

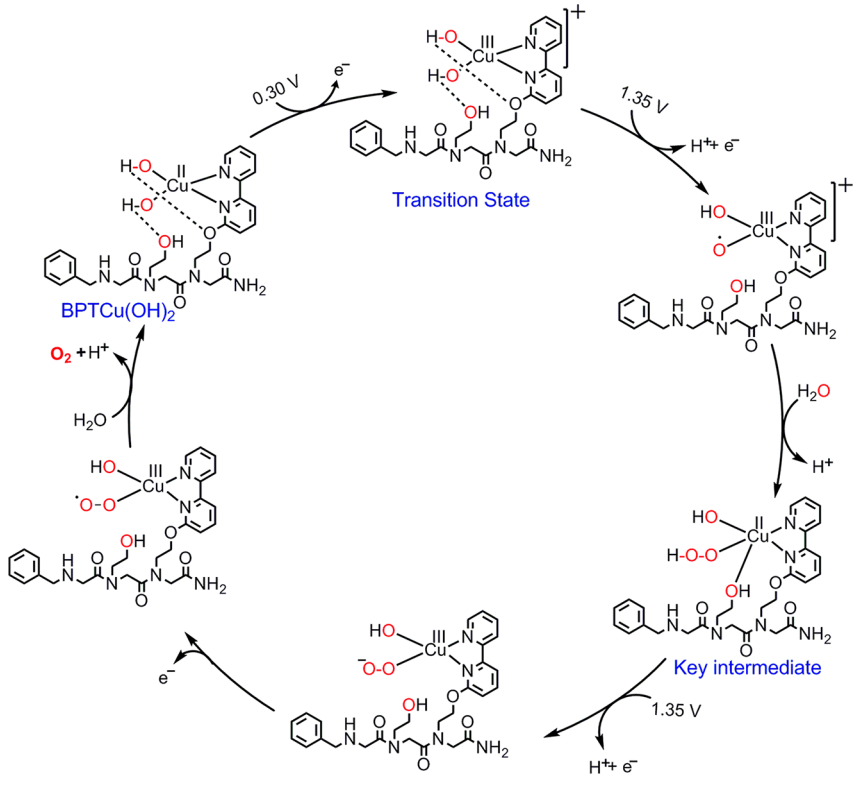

DOI: 10.1021/acscatal.8b03661
ACS Catal. 2018, 8, 10631−10640

$$\frac{i}{i_p^0} = \frac{2.24\sqrt{\frac{RT}{Fv}\cdot 2kC_A^0}}{1 + \exp\left[\frac{F}{RT}(E - E^0)\right]} \quad \text{(iii)}$$

From plotting $i/i_p{}^0$ versus $1/\{1 + \exp[F/RT\ (E - E^0)]\}$, it is possible to draw a straight line, which represents the very beginning of the catalytic process, with a slope of $2.24\{(RT/Fv)^{1/2}\}\cdot(2kC_A{}^0)^{1/2}$ that gives immediate access to $2k$ and therefore to the TOF and TON. Applying these equations to our catalytic system (see Figure S22) gives an average value of $k_{obs} = 5.80\ s^{-1}$, which is independent of the scan rate.

At this point, we wanted to understand the high stability and activity of our catalyst and to suggest a reasonable explanation for it. On the basis of the low potential required for the $Cu^{II/III}$ oxidation and the hydrogen bonding shown in the calculated structure of [**BPT**$Cu^{II}(OH)_2$], we assumed that the ethanolic−OH group has a role in the catalytic mechanism and there might be some cooperativity between the copper center and the peptoid. Previous mechanistic studies on a Cu-based water oxidation electrocatalyst, reported by Meyer et al., suggested that water oxidation occurs via the formation of an O−O bond and a key Cu-peroxo intermediate, which is formed due to an oxygen atom transfer from a water molecule coupled with a proton loss.[8b] Based on these studies, as well as on our experimental data and theoretical calculations, we have proposed a plausible mechanism, which is depicted in Scheme 2. We propose that in the first step, at potential 0.30 V, the complex [**BPT**$Cu^{III}(OH)_2]^+$, which is stabilized by hydrogen bonding, is formed. Thereafter, at a potential of 1.35 V vs. NHE, further oxidation of [**BPT**$Cu^{III}(OH)_2]^+$ occurs, with an additional proton and electron loss to form the highly unstable transition state [**BPT**$Cu^{III}(\dot{O})(OH)]^+$. Once formed, this undergoes rate-limiting O−O bond formation by reaction with a water molecule to give a hydroperoxide [**BPT**$Cu^{II}(OOH)(OH)$] as a key intermediate in the reaction. This intermediate can be further stabilized by a bond formation between the ethanolic −OH group and copper, leading to a preferred penta-coordinated geometry about the Cu center.[24] The catalytic peak current at 1.35 V versus NHE normalized by the inverse square root of the scan rate (i_c/i_d vs $v^{-1/2}$) in Figure S23, increases with a decrease in the scan rate, consistent with a chemical step and rate limiting bond formation.[8b] The irreversibility of the second oxidation results from further oxidation of the intermediate peroxide, [**BPT**$Cu^{III}(OO^-)(OH)$], assisted by another proton abstraction, resulting in the formation of [**BPT**$Cu^{III}(O\dot{O})(OH)$], which finally leads to the release of O_2 and to the reentry of [**BPT**$Cu^{II}(OH)_2$] into the catalytic cycle.

In attempts to provide experimental evidence for the proposed peroxide intermediate, we performed a CV experiment in the presence of H_2O_2. Upon addition of hydrogen peroxide solution to a buffer solution containing [**BPT**$Cu^{II}(OH)_2$] with scan reversal before the catalytic water oxidation, a new wave appears at $E = -0.40$ V (Figure S24, red and green lines). This is the same wave that appears when scanning through the catalytic wave at 1.35 V vs. NHE at the same pH and scan rate conditions (pH 11.5 and 100 mV/s scan rate) in the presence of [**BPT**$Cu^{II}(OH)_2$] but in the absence of hydrogen peroxide (Figure S24, blue line). Thus, this wave can be assigned to the reduction of a peroxo intermediate. However, this wave can also be assigned to the reduction of O_2, which is formed in this reaction. Therefore, this experiment did not provide an evidence for the formation of a peroxo intermediate. Consequently, we have performed additional UV−vis titration and spectroelectrochemistry experiments under N_2 atmosphere. First, we titrated the catalyst with added aliquots of 6% H_2O_2 sequentially and observed a significant decay of the band near 322 nm, together with the appearance of a new band near 248 nm (Figure 6a).

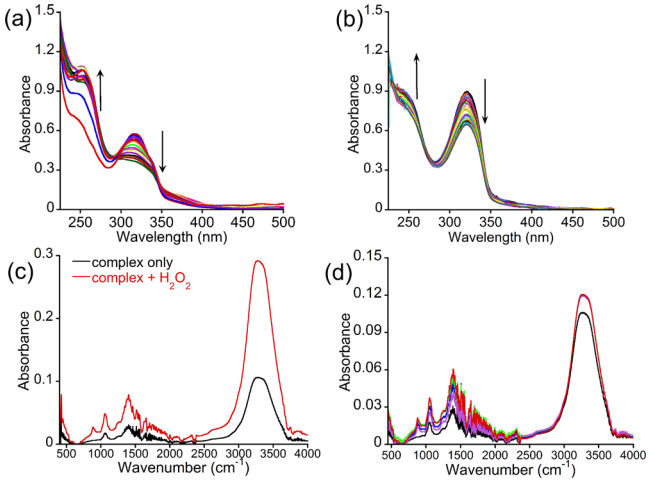

Figure 6. (a) Titration of 60 μM [**BPT**$Cu(OH)_2$] with aliquots of 2 μL of 6% H_2O_2 followed by UV−vis spectroscopy. (b) UV−vis spectroscopy of 80 μM [**BPT**$Cu(OH)_2$] during spectroelectrochemistry experiment done under N_2 atmosphere at an applied potential of 1.35 V vs NHE. (c) IR spectra of [**BPT**$Cu(OH)_2$] (1 mM, 1 mL) complex after addition of few drops of 2% H_2O_2. (d) IR spectra of [**BPT**$Cu(OH)_2$] (1 mM, 5 mL complex during electrolysis at 1.35 V vs NHE. All the experiments were done in 0.1 M phosphate buffer at pH 11.5 and at room temperature.

To identify this new band, we have subjected this solution to ESI-MS analysis and this showed mass at 634.65 and 636.17, corresponding to the mass of the proposed penta-coordinated peroxo species as the key intermediate (Figure S27).

Thereafter, we measured the spectroelectrchemistry of the catalyst without added H_2O_2, by applying continues potential at 1.35 V versus NHE. This experiment showed similar changes in the UV−vis spectrum at 322 and 248 nm (Figure 6b), clearly indicating that the species generated during electrolysis is the peroxo bound species.

EPR analysis of [**BPT**$Cu^{II}(OH)_2$] during catalysis in basic phosphate buffer solution (0.5 mM, frozen sample) resulted in a spectrum that is characteristic of a Cu (II) system. The simulated spectrum produced the parameters g|| = 2.231, g⊥ = 2.092 and A|| = 160 G (Figure S28), which suggest a penta-coordinated Cu ion via 3O and 2N atoms.[16] An EPR measurement performed after addition of 20 μL of 6% H_2O_2 solution to the 0.5 mM [**BPT**$Cu^{II}(OH)_2$] complex in phosphate buffer solution (frozen sample) led to a similar spectrum, which its simulation produced the parameters g|| = 2.214, g⊥ = 2.076 and A|| = 167 G (Figure S29). These results are consistent with those obtained from the spectrum of the sample taken from the catalytic experiment, suggesting a penta-coordinated Cu ion via 3O and 2N atoms and providing another support for the formation of the peroxo-complex during catalysis. In addition, we have performed the spectroelectrochemistry IR measurements of the 0.5 mM [**BPT**$Cu^{II}(OH)_2$] catalyst in 0.1 M phosphate buffer solution. The IR spectrum showed the generation of a new band at 876 cm^{-1} during electrolysis (Figure 6d), which is the characteristic

DOI: 10.1021/acscatal.8b03661
ACS Catal. 2018, 8, 10631−10640

band of υ(O−O) stretch.[25] These results were further supported by a similar IR measurement performed after H_2O_2 was directly added to the catalyst solution, which showed the generation of a new band at 880 cm^{-1} (Figure 6c). All the IR spectra were measured at room temperature. These IR analyses provide another strong indication that the electrochemically generated active species during catalysis is the peroxo species.

The formation of the peroxo key intermediate was also corroborated by computational calculations. Thus, the catalyst [**BPT**$Cu^{II}(OH)_2$], one crucial transition state, [**BPT**$Cu^{III}(OH)_2]^+$, and the key intermediate state [**BPT**Cu^{II}(OH)(OOH)] have been optimized by the theoretical DFT-D3 analysis using turbomole and ORCA (3.0.3) software package (see Figure 7 and Table S3−S5 in SI file for the coordinates). DFT-D3 (considering the dispersion correction)[18] has been utilized at the level of B3-LYP hybrid functional. def2-SVP has been used as basis sets for carbon, nitrogen, oxygen, and hydrogen atoms. In case of Cu^{II} center, triple-ζ basis set (i.e., def2-TZVP) is used. The solvent model COSMO for water is utilized to accurately mimic the reaction vessel. In each case, the grid size during geometry optimization has been chosen as m5, where the accuracy level would be high with 10^{-9} au SCF convergence.[26] Following the optimization of [**BPT**$Cu^{II}(OH)_2$], the transition state [**BPT**Cu^{III}(OH)-(OH)]$^+$ has been optimized. The optimized geometry revealed a tetra-coordinated Cu^{III} complex. The energy of this complex is only slightly higher than this of [**BPT**$Cu^{II}(OH)_2$] (Figure 7 (2)). The distances between coordinated atoms and the Cu center are as follows: Cu (1)-N(7): 2.04 Å, Cu(1)−N(8): 2.10 Å, Cu(1)−O(41): 1.91 Å, Cu(1)−O(40): 1.86 Å. The angles are O(41)−Cu(1)−N(7): 92.90°, O(40)−Cu(1)−N(8): 99.54°, N(7)−Cu(1)−N(8): 79.07°, O(40)−Cu(1)−O(41): 96.31°. Furthermore, the key intermediate in the reaction mechanism, [**BPT** Cu^{II}(OH)(OOH)], has been optimized at the same level of DFT-D3. The optimized geometry implies that the central metal is penta-coordinated[24] (Figure 7 (3)), and the bond distances of the ligated centers from the central metal are as follows: Cu (1)-N(7): 2.08 Å, Cu(1)−N(8): 2.22 Å, Cu(1)−O(41): 1.96 Å, Cu(1)−O(40): 1.87 Å and Cu(1)−O(4): 2.25 Å. The angles are O(41)−Cu(1)−N(7): 91.73°, O(40)−Cu(1)−N(8): 100.77°, N(7)−Cu(1)−N(8): 76.60°, O(40)−Cu(1)−O(41): 94.65°, O(4)−Cu(1)−O(41): 86.05°, O(4)−Cu(1)−O(40): 118.2°, O(4)−Cu(1)−N(8): 84.43°, O(4)−Cu(1)−N(7): 93.89°. The energy of the key intermediate is lower than the original complex by ∼1.96 × 10^5 kJ/mol, which suggests that the reaction could proceed forward according to the proposed path depicted in Scheme 2. For further insight, single point energy calculation of each geometry value has been executed at higher level by def2-TZVP basis set for all atoms. At this higher level of calculation, we obtained a similar trend, *i.e.;* the transition state [**BPT**$Cu^{III}(OH)_2]^+$ is energetically higher than [**BPT**$Cu^{II}(OH)_2$]. On the other hand, the key intermediate is energetically lower than [**BPT**$Cu^{II}(OH)_2$] by ∼1.97 × 10^5 kJ/mol. The energy values are mentioned in the SI file. Also, the Gibbs free energy for [**BPT**$Cu^{II}(OH)_2$] and [**BPT**Cu^{II}(OH)(OOH)] has been calculated at 298.15K and found as −93.1 and −94.01 kJ/mol, respectively.

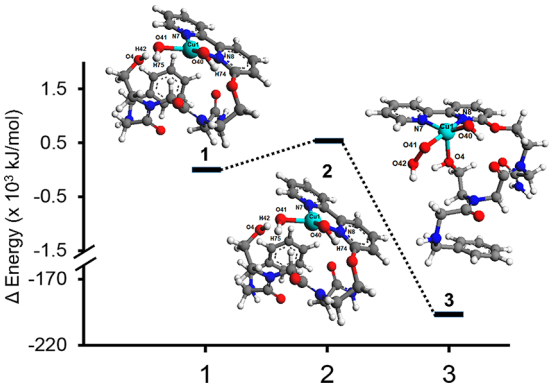

Figure 7. Geometry optimized structure of the (1) complex [**BPT**$Cu^{II}(OH)_2$], (2) transition state [**BPT**Cu^{III}(OH)(OH)]$^+$, and (3) key intermediate [**BPT**Cu^{II}(OH)(OOH)] by DFT-D3 method.

Therefore, the formation of the stable key peroxo intermediate via the increase in the coordination number of the Cu ion is supported by both experimental (see Figure 6) and theoretical characterization.[24] These results suggest that the incorporation of an $-CH_2CH_2OH$ group next to the bipy group on the same peptoid scaffold has a significant role in the high stability of the catalyst, which is also responsible for its high activity. The presence of a flexible −OH group next to the active metal center facilitates the oxidation process and stabilizes both the transition state and the key intermediates formed in the reaction. This indicates a cooperative mechanism similar to enzymatic mode of action, in which the copper center oxidizes the water, while the noncatalytic side chain −OH group assists the oxidation and stabilizes the active species. Overall, this cooperativity leads to a highly stable water oxidation catalyst that can function continuously (given the pH level is kept constant) without any loss of its activity.

CONCLUSIONS

Disclosed here is the first example of a copper peptoid complex, which successfully functions as a robust, homogeneous electrocatalyst for water oxidation with a key intermediate characterized. Although water oxidation occurs at a high overpotential of 800 mV at pH 11.5 in 0.1 M phosphate buffer, the rate, turnover numbers, and the catalyst stability are impressive. The stability of the catalyst, the key intermediate, and the peptoid ligand in alkaline buffer solution during water electrolysis are notable because this leads to a highly efficient catalytic system, which can be reused over and over again without loss of activity, thus enabling to significantly increase the overall TON. We advocate that this high stability is a consequence of an enzymatic-like intramolecular cooperativity between the noncatalytic peptoid side-chain −OH group and the nearby catalytic copper center, located on the same scaffold. The demonstration of such cooperativity, that is, facilitated within peptidomimetic scaffolds, in which the type and the number of metal-binding ligands and proton acceptors, as well as their position along the backbone can be easily varied and tuned, enables the investigation of various peptide mimics as water oxidation catalysts. We are currently working toward improving the catalytic performance of this system, aiming to reduce its overpotential and increase its rate, by systematically modifying its sequence, along with the development of new metallopeptoids as efficient catalysts for water electrolysis and photolysis.

DOI: 10.1021/acscatal.8b03661
ACS Catal. 2018, 8, 10631−10640

EXPERIMENTAL SECTION

Preparation and Characterization of BPT. Peptoid **BPT** (Scheme 1) was synthesized manually on Rink amide resin using the sub monomer approach at room temperature and was characterized by analytical HPLC and ESI MS analysis, as previously reported.[15] The peptoid was further purified to >95% by RP-HPLC and lyophilized overnight. HPLC trace and MS spectrum of the pure peptoid are depicted in Figures S1 and S2, respectively.

Synthesis and Characterization of the Complex [BPTCu^{II}(OH)$_2$]. The peptoid **BPT** (0.1 mmol) was dissolved in methanol (1 mL), and the mixture was stirred for 10 min. This mixture was treated with copper perchlorate hexahydrate (0.1 mmol as solid) and stirred for another 2 h. A blue-colored solid precipitate was obtained and was isolated by centrifugation, washed twice with methanol, and lyophilized overnight. Then the solid compound was dissolved in water and basic phosphate buffer solution and characterized by ESI-MS (Figure S4), FT-IR (Figure S5), UV−vis (Figure S6), and EPR spectroscopy (Figure S7).

Kinetic Analysis by Foot of the Wave (FOWA) and TON Calculation. This methodology was implied assuming that the rate-determining step (rds) is the O−O bond formation by reaction with water molecule to give a hydroperoxide intermediate [Cu^{II}(OOH)] directly. Under catalytic conditions, the relevant equation is as follows:

$$\frac{i_{cat}}{i_d} = \frac{n \cdot 2.24 \cdot \sqrt{\frac{RT}{Fv}} \cdot k_{obs}}{1 + \exp\left[\frac{F}{RT}(E^0_{cat} - E)\right]}$$

E^0_{cat} is the standard potential for the catalysis-initiating redox couple (1.35 V calculated from DPV, Figure S8), i_{cat} is the current intensity in the presence of substrate, i_d is the current intensity in the absence of substrate (here we approximate this current to the current associated with the Cu^{II} /Cu^{III} couple), n is the number of electrons involved in the catalytic cycle (4 e$^-$ in water oxidation), F is the faraday constant, υ is the scan rate, k_{obs} is defined as "$k_{cat}\cdot C^0_A$" where C^0_A is the concentration of substrate (55.56 M for water), and R is 8.314 J·mol^{-1} K^{-1}. Background corrected CVs of catalyst at different scan rates (2−100 mVs^{-1}). Now, k_{obs} can be extracted from the plot of i_c/i_d versus $1/(1 + \exp[(F/RT)(E^0_{cat} - E)])$. So from the graph the obtained k_{obs} value for the catalysis is 5.80 s^{-1}. According to Saveant and co-workers, the TON for electrolytic water oxidation can be obtained from the following equation:[12]

$$\mathrm{TON} = \frac{k_{cat} \times t}{1 + \exp\left[-\frac{F}{RT}(E - E^0)\right]}$$

The calculated TON considering the FOWA is 41 760 in 2 h.

Calculation of Faradaic Efficiency from Total Charge Accumulated during Control Potential Electrolysis (CPE). Faradaic efficiency FE (%) was calculated based on following equation:

$$\mathrm{FE}\ (\%) = \frac{4 \times \text{amount of } O_2\ (\text{moles}) \times 100}{n\ (\text{moles of electrons})}$$

where

$$n = \frac{Q\ (\text{columb})}{F\ (\text{Faradayconst.})}$$

Here, the amount of O_2 produced in 2 h of electrolysis was 22.5×10^{-6} mol (total O_2 produced in 2 h = 115 μM = 550 μL, obtained from calibration curve in Figure S31), and the total accumulated charge during 2 h of electrolysis was 9.5C (after blank subtraction), and as F = 96485.33C the Faradaic Efficiency of the electro catalysis reaction in 2 h is 91%.

ASSOCIATED CONTENT

Supporting Information

The Supporting Information is available free of charge on the ACS Publications website at DOI: 10.1021/acscatal.8b03661.

Experimental details, mass spectroscopy, DFT calculations details and all electrochemical, spectroscopic and chromatography details, and calculations for TON, TOF, and faradic efficiency (PDF)

AUTHOR INFORMATION

Corresponding Author

*E-mail: gm92@technion.ac.il.

ORCID

Pritam Ghosh: 0000-0002-2345-8036

Galia Maayan: 0000-0001-5711-7339

Author Contributions

The manuscript was written through contributions of all authors. All authors have given approval to the final version of the manuscript.

Funding

This research was funded by the Solar Fuels Israel Center of Research Excellence (I-CORE) of the Israeli Science Foundation (ISF), grant number 2018762, and was supported by the Grand Technion Energy Program.

Notes

The authors declare no competing financial interest.

ACKNOWLEDGMENTS

The authors thank Dr. Boris Tumanskii from the Schulich Faculty of Chemistry for the EPR spectra measurements and simulations.

REFERENCES

(1) (a) Wang, D.; Marquard, S. L.; Troian-Gautier, L.; Sheridan, M. V.; Sherman, B. D.; Wang, Y.; Eberhart, M. S.; Farnum, B. H.; Dares, C. J.; Meyer, T. J. Interfacial Deposition of Ru(II) Bipyridine-Dicarboxylate Complexes by Ligand Substitution for Applications in Water Oxidation Catalysis. *J. Am. Chem. Soc.* **2018**, *140*, 719−726. (b) Nocera, D. G. Solar Fuels and Solar Chemicals Industry. *Acc. Chem. Res.* **2017**, *50*, 616−619. (c) Wu, L. Z.; Chen, B.; Li, Z. J.; Tung, C. H. Enhancement of the Efficiency of Photocatalytic Reduction of Protons to Hydrogen via Molecular Assembly. *Acc. Chem. Res.* **2014**, *47*, 2177−2185.

(2) Hunter, B. M.; Gray, H. B.; Müller, A. M. Earth-Abundant Heterogeneous Water Oxidation Catalysts. *Chem. Rev.* **2016**, *116*, 14120−14136.

(3) Wang, Y.; Suzuki, H.; Xie, J.; Tomita, O.; Martin, D. J.; Higashi, M.; Kong, D.; Abe, R.; Tang, J. Mimicking Natural Photosynthesis: Solar to Renewable H_2 Fuel Synthesis by Z-Scheme Water Splitting Systems. *Chem. Rev.* **2018**, *118*, 5201−5241.

(4) (a) Ye, S.; Ding, C.; Chen, R.; Fan, F.; Fu, P.; Yin, H.; Wang, X.; Wang, Z.; Du, P.; Li, C. Mimicking the Key Functions of Photosystem II in Artificial Photosynthesis for Photoelectrocatalytic Water Splitting. *J. Am. Chem. Soc.* **2018**, *140*, 3250−3256. (b) You, B.; Sun, Y. Innovative Strategies for Electrocatalytic Water Splitting. *Acc. Chem. Res.* **2018**, *51*, 1571−1580.

DOI: 10.1021/acscatal.8b03661
ACS Catal. 2018, 8, 10631−10640

(5) (a) Wasylenko, D. J.; Ganesamoorthy, C.; Borau-Garcia, J.; Berlinguette, C. P. Electrochemical Evidence for Catalytic Water Oxidation Mediated by a High-Valent Cobalt Complex. *Chem. Commun.* **2011**, *47*, 4249−4251. (b) Dogutan, D. K.; McGuire, R.; Nocera, D. G. Electocatalytic Water Oxidation by Cobalt(III) Hangman B-Octafluoro Corroles. *J. Am. Chem. Soc.* **2011**, *133*, 9178−9180.

(6) (a) Ellis, W. C.; Mcdaniel, N. D.; Bernhard, S.; Collins, T. J. Fast Water Oxidation Using Iron. *J. Am. Chem. Soc.* **2010**, *132*, 10990−10991. (b) Fillol, J. L.; Codolà, Z.; Garcia-Bosch, I.; Gomez, L.; Pla, J. J.; Costas, M. Efficient Water Oxidation Catalysts Based on Readily Available Iron Coordination Complexes. *Nat. Chem.* **2011**, *3*, 807−813.

(7) (a) Zhang, M.; Zhang, M. T.; Hou, C.; Ke, Z. F.; Lu, T. B. Homogeneous Electrocatalytic Water Oxidation at Neutral pH by a Robust Macrocyclic Nickel(II) Complex. *Angew. Chem., Int. Ed.* **2014**, *53*, 13042−13048. (b) Han, Y.; Wu, Y.; Lai, W.; Cao, R. Electrocatalytic Water Oxidation by a Water-Soluble Nickel Porphyrin Complex at Neutral pH with Low Overpotential. *Inorg. Chem.* **2015**, *54*, 5604−5613.

(8) (a) Barnett, S. M.; Goldberg, K. I.; Mayer, J. M. A Soluble Copper−Bipyridine Water- Oxidation Electrocatalyst. *Nat. Chem.* **2012**, *4*, 498−502. (b) Zhang, M. T.; Chen, Z.; Kang, P.; Meyer, T. J. Electrocatalytic Water Oxidation with a Copper(II) Polypeptide Complex. *J. Am. Chem. Soc.* **2013**, *135*, 2048−2051. (c) Garrido-Barros, P.; Funes-Ardoiz, I.; Drouet, S.; Benet-Buchholz, J.; Maseras, F.; Llobet, A. Redox Non-Innocent Ligand Controls Water Oxidation Overpotential in a New Family of Mononuclear Cu-Based Efficient Catalysts. *J. Am. Chem. Soc.* **2015**, *137*, 6758−6761.

(9) Maayan, G.; Gluz, N.; Christou, G. A Bioinspired Soluble Manganese Cluster as a Water Oxidation Electrocatalyst with Low Overpotential. *Nat. Catal.* **2018**, *1*, 48−54.

(10) (a) Coggins, M. K.; Zhang, M. T.; Chen, Z.; Song, N.; Meyer, T. J. Single-Site Copper(II) Water Oxidation Electrocatalysis: Rate Enhancements With HPO_4^{2-} as a Proton Acceptor at PH 8. *Angew. Chem., Int. Ed.* **2014**, *53*, 12226−12230. (b) Su, X. J.; Gao, M.; Jiao, L.; Liao, R. Z.; Siegbahn, P. E. M.; Cheng, J. P.; Zhang, M. T. Electrocatalytic Water Oxidation by a Dinuclear Copper Complex in a Neutral Aqueous Solution. *Angew. Chem., Int. Ed.* **2015**, *54*, 4909−4914. (c) Fisher, K. J.; Materna, K. L.; Mercado, B. Q.; Crabtree, R. H.; Brudvig, G. W. Electrocatalytic Water Oxidation by a Copper(II) Complex of an Oxidation-Resistant Ligand. *ACS Catal.* **2017**, *7*, 3384−3387. (d) Liu, X.; Jia, H.; Sun, Z.; Chen, H.; Xu, P.; Du, P. Nanostructured Copper Oxide Electrodeposited From Copper(II) Complexes as an Active Catalyst for Electrocatalytic Oxygen Evolution Reaction. *Electrochem. Commun.* **2014**, *46*, 1−4. (e) Fu, L. Z.; Fang, T.; Zhou, L. L.; Zhan, S. Z. A Mononuclear Copper Electrocatalyst for Both Water Reduction and Oxidation. *RSC Adv.* **2014**, *4*, 53674−53680. (f) Gerlach, D. L.; Bhagan, S.; Cruce, A. A.; Burks, D. B.; Nieto, I.; Truong, H. T.; Kelley, S. P.; Herbst-Gervasoni, C. J.; Jernigan, K. L.; Bowman, M. K.; Pan, S.; Zeller, M.; Papish, E. T. Studies of the Pathways Open to Copper Water Oxidation Catalysts Containing Proximal Hydroxy Groups During Basic Electrocatalysis. *Inorg. Chem.* **2014**, *53*, 12689−12698. (g) Yu, W. B.; He, Q. Y.; Ma, X. F.; Shi, H. T.; Wei, X. A New Copper Species Based on an Azo-Compound Utilized as a Homogeneous Catalyst for Water Oxidation. *Dalt. Trans.* **2015**, *44*, 351−358. (h) Li, T. T.; Cao, S.; Yang, C.; Chen, Y.; Lv, X. J.; Fu, W. F. Electrochemical Water Oxidation by in Situ-Generated Copper Oxide Film From $[Cu(TEOA)(H_2O)_2][SO_4]$ Complex. *Inorg. Chem.* **2015**, *54*, 3061−3067. (i) Pap, J. S.; Szyrwiel, Ł.; Srankó, D.; Kerner, Z.; Setner, B.; Szewczuk, Z.; Malinka, W. Electrocatalytic Water Oxidation by Cu^{II} Complexes with Branched Peptides. *Chem. Commun.* **2015**, *51*, 6322−6324. (j) Chen, Z.; Meyer, T. J. Copper(II) Catalysis of Water Oxidation. *Angew. Chem., Int. Ed.* **2013**, *52*, 700−703. (k) Yu, F.; Li, F.; Zhang, B.; Li, H.; Sun, L. Efficient Electrocatalytic Water Oxidation by a Copper Oxide Thin Film in Borate Buffer. *ACS Catal.* **2015**, *5*, 627−630.

(11) Zhang, T.; Wang, C.; Liu, S.; Wang, J. L.; Lin, W. A Biomimetic Copper Water Oxidation Catalyst with Low Overpotential. *J. Am. Chem. Soc.* **2014**, *136*, 273−281.

(12) (a) Baskin, M.; Maayan, G. Water-Soluble Chiral Metallopeptoids. *Biopolymers* **2015**, *104*, 577−584. (b) De Cola, C.; Fiorillo, G.; Meli, A.; Aime, S.; Gianolio, E.; Izzo, I.; De Riccardis, F. Gadolinium-Binding Cyclic Hexapeptoids: Synthesis and Relaxometric Properties. *Org. Biomol. Chem.* **2014**, *12*, 424−431. (c) Sala, G. D.; Nardone, B.; De Riccardis, F.; Izzo, I. Cyclopeptoids: A Novel Class of Phase-Transfer Catalysts. *Org. Biomol. Chem.* **2013**, *11*, 726−731. (d) Izzo, I.; Ianniello, G.; De Cola, C.; Nardone, B.; Erra, L.; Vaughan, G.; Tedesco, C.; De Riccardis, F. Structural Effects of Proline Substitution and Metal Binding on Hexameric Cyclic Peptoids. *Org. Lett.* **2013**, *15*, 598−601. (e) Maayan, G.; Ward, M. D.; Kirshenbaum, K. Metallopeptoids. *Chem. Commun.* **2009**, 56−58. (f) Baskin, M.; Panz, L.; Maayan, G. Versatile Ruthenium Complexes Based on 2,2′-Bipyridine Modified Peptoids. *Chem. Commun.* **2016**, *52*, 10350−10353. (g) Baskin, M.; Maayan, G. A Rationally Designed Metal-Binding Helical Peptoid for Selective Recognition Processes. *Chem. Sci.* **2016**, *7*, 2809−2820. (h) Schettini, R.; De Riccardis, F.; Della Sala, G.; Izzo, I. Enantioselective Alkylation of Amino Acid Derivatives Promoted by Cyclic Peptoids under Phase-Transfer Conditions. *J. Org. Chem.* **2016**, *81*, 2494−2505. (i) Maayan, G.; Ward, M. D.; Kirshenbaum, K. Folded Biomimetic Oligomers for Enantioselective Catalysis. *Proc. Natl. Acad. Sci. U. S. A.* **2009**, *106*, 13679−13684. (j) Zabrodski, T.; Baskin, M.; Kaniraj, J. P.; Maayan, G. Click To Bind: Microwave Assisted Solid-Phase Synthesis of Peptoids Incorporating Pyridine-Triazole Ligands and their Copper-(II) Complexes. *Synlett* **2015**, *26*, 461−466. (k) Zborovsky, L.; Smolyakova, A.; Baskin, M.; Maayan, G. A Pure Polyproline Type I-like Peptoid Helix via Metal Coordination. *Chem. - Eur. J.* **2018**, *24*, 1159−1167. (l) Baskin, M.; Maayan, G. Chiral Cu(II), Co(II) And Ni(II) Complexes Based on 2,2′-Bipyridine Modified Peptoids. *Dalton Trans.* **2018**, *47*, 10767−10774. (m) Maayan, G.; Liu, L.-K. Silver Nanoparticles Assemblies Mediated by Functionalized Biomimetic Oligomers. *Biopolymers* **2011**, *96*, 679−687.

(13) (a) Mohan, D. C.; Sadhukha, A.; Maayan, G. A Metallopeptoid as an Efficient Bioinspired Cooperative Catalyst for the Aerobic Oxidative Synthesis of Imines. *J. Catal.* **2017**, *355*, 139−144. (b) Prathap, K. J.; Maayan, G. Metallopeptoids as Efficient Biomimetic Catalysts. *Chem. Commun.* **2015**, *51*, 11096−11099.

(14) Kaniraj, P. J.; Maayan, G. A Facile Strategy for The Construction of Cyclic Peptoids under MW Irradiation through a Simple Substitution Reaction. *Org. Lett.* **2015**, *17*, 2110−2113.

(15) Ghosh, T.; Fridman, N.; Kosa, M.; Maayan, G. Self-Assembled Cyclic Structures from Copper (II) Peptoid. *Angew. Chem., Int. Ed.* **2018**, *57*, 7703−7708.

(16) (a) Peisach, J.; Blumberg, W. E. Structural Implications Derived from the Analysis of Electron Paramagnetic Resonance Spectra of Natural and Artificial Copper Proteins. *Arch. Biochem. Biophys.* **1974**, *165*, 691−708. (b) Baskin, M.; Fridman, N.; Kosa, M.; Maayan, M. Heteroleptic Complexes via Solubility Control: Examples of Cu(II), Co(II), Ni(II) and Mn(II) Complexes Based on the Derivatives of Terpyridine and Hydroxyquinoline. *Dalton Trans.* **2017**, *46*, 15330−15339.

(17) (a) Fabian, I. Hydrolytic Reactions of Copper(II) Bipyridine Complexes. *Inorg. Chem.* **1989**, *28*, 3805−3807. (b) Garribba, E.; Micera, G.; Sanna, D.; Strinna-Erre, L. The Cu (II)-2, 2′-Bipyridine System Revisited. *Inorg. Chim. Acta* **2000**, *299*, 253−261.

(18) (a) Grimme, S. Supramolecular Binding Thermodynamics by Dispersion-Corrected Density Functional Theory. *Chem. - Eur. J.* **2012**, *18*, 9955−9964. (b) Grimme, S.; Ehrlich, S.; Goerigk, L. Effect of the Damping Function in Dispersion Corrected Density Functional Theory. *J. Comput. Chem.* **2011**, *32*, 1456−1465.

(19) Bard, A. J.; Faulkner, L. R. *Electrochemical Methods: Fundamentals and Applications*; John Wiley & Sons, Inc.: Hoboken, NJ, 1944.

(20) Creus, J.; Matheu, R.; Penafiel, I.; Moonshiram, D.; Blondeau, P.; Benet-Buchholz, J.; Garcia-Anton, J.; Sala, X.; Godard, C.; Llobet,

DOI: 10.1021/acscatal.8b03661
ACS Catal. 2018, 8, 10631−10640

A. A Million Turnover Molecular Anode for Catalytic Water Oxidation. *Angew. Chem., Int. Ed.* **2016**, *55*, 15382−15386.
(21) Costentin, C.; Drouet, S.; Robert, M.; Saveant, J. M. Turnover Numbers, Turnover Frequencies, and Overpotential in Molecular Catalysis of Electrochemical Reactions. Cyclic Voltammetry and Preparative-Scale Electrolysis. *J. Am. Chem. Soc.* **2012**, *134*, 11235−11242.
(22) (a) Saveant, J. M. Molecular Catalysis of Electrochemical Reactions. Mechanistic Aspects. *Chem. Rev.* **2008**, *108*, 2348−2378. (b) Savéant, J. M.; Su, K. B. Homogeneous Redox Catalysis of Electrochemical Reaction. *J. Electroanal. Chem. Interfacial Electrochem.* **1984**, *171*, 341−349. (c) Saveant, J. M.; Vianello, E. Potential-Sweep Chronoamperometry: Kinetic Currents for First-Order Chemical Reaction Parallel to Electron-Transfer Process (Catalytic Currents). *Electrochim. Acta* **1965**, *10*, 905−920.
(23) Savéant, J. M. *Elements of Molecular and Biomolecular Electrochemistry: An Electrochemical Approach to Electron Transfer Chemistry*; John Wiley & Sons, Inc.: Hoboken, NJ, 2000.
(24) (a) Itoh, S. Mononuclear Copper Active-Oxygen Complexes. *Curr. Opin. Chem. Biol.* **2006**, *10*, 115−122. (b) Fujii, T.; Yamaguchi, S.; Funahashi, Y.; Ozawa, T.; Tosha, T.; Kitagawa, T.; Masuda, H. Mononuclear Copper (II)−Hydroperoxo Complex Derived from Reaction of Copper (I) Complex with Dioxygen as a Model of Dbm and PHM. *Chem. Commun.* **2006**, 4428−4430. (c) Kim, S.; Saracini, C.; Siegler, M. A.; Drichko, N.; Karlin, K. D. Coordination Chemistry and Reactivity of a Cupric Hydroperoxide Species Featuring a Proximal H-Bonding Substituent. *Inorg. Chem.* **2012**, *51*, 12603−12605.
(25) (a) Root, D. E.; Mahroof-Tahir, M.; Karlin, K. D.; Solomon, E. I. Effect of Protonation On Peroxo-Copper Bonding: Spectroscopic and Electronic Structure Study of $[Cu_2((UN\text{-}O\text{-})(OOH)]^{2+}$. *Inorg. Chem.* **1998**, *37*, 4838−4848. (b) Campbell, N. J.; Dengel, A. C.; Griffith, W. P. Studies on Transition Metal Peroxo Complexes-X. The Nature of Peroxovanadates in Aqueous Solution. *Polyhedron* **1989**, *8*, 1379−1386.
(26) Eichkorn, K.; Weigend, F.; Treutler, O.; Ahlrichs, R. Auxiliary Basis Sets for Main Row Atoms and Transition Metals and Their Use to Approximate Coulomb Potentials. *Theor. Chem. Acc.* **1997**, *97*, 119−124.

DOI: 10.1021/acscatal.8b03661
ACS Catal. 2018, 8, 10631−10640